JOURNAL OF MATERIALS SCIENCE 12 (1977) 1039–1049

The structure of amorphous aluminium phosphate by radial distribution functions derived from X-ray diffraction

G. D. WIGNALL
ICI Europa Limited, Everslaan, 45 B 3078 Everberg, Belgium

R. N. ROTHON, G. W. LONGMAN, G. R. WOODWARD
ICI Mond Division, Research and Development Department and ICI Corporate Laboratory, The Heath, Runcorn, Cheshire, UK

An investigation of the molecular structure of amorphous aluminium phosphate, prepared from a recently discovered complex ($AlPO_4 \cdot HCl \cdot 4C_2H_5OH$), has been carried out using radial distribution function (RDF) techniques. Studies were made on two samples, one prepared by decomposing the solid complex and the other from powder produced by evaporating to dryness a solution of the complex in methanol and then decomposing and grinding the solid obtained. RDF curves were obtained from both samples, and were found to closely resemble that previously reported for vitreous silica. The short range order in both samples is similar to that in vitreous silica, with aluminium and phosphorous atoms occupying positions in aluminium phosphate similar to the positions of silicon atoms in silica. This structure is consistent with the crystal chemistry of aluminium phosphate.

It is possible to assign all the peaks in the RDF plots out to values of $r \sim 5$ Å to known inter-atomic distances. The peak at 1.6 Å represents the Al–O and Al–P bond lengths, and is broader than the corresponding Si–O peak in vitreous silica, as the Al–O and P–O bonds are respectively slightly longer (Al–O) and shorter (P–O) than the equivalent Si–O bonds. Subsequent peaks result from the O–O distances (~ 2.6 Å); the Al–Al, Al–P and P–P distances (~ 3.1 Å); the Al–second O and P–second O distances (~ 4.2 Å), and O–second O, Al–second Al, P–second P and Al–second P distances (~ 5.0 Å). The sample prepared from the methanolic solution shows some small additional peaks in the region 4 to 5 Å, indicating more order in the second neighbour distances.

Analysis of the P–O and Al–O peak area indicates that both P and Al atoms are co-ordinated to four network oxygen atoms at a distance ~ 1.6 Å, and that absorbed water also co-ordinates to one or both atoms with a P–O and/or Al–O distance of ~ 1.6 Å.

1. Introduction

A number of metal complexes, mainly phosphate based, have been discovered which possess interesting properties as surface coating agents [1]. The coatings are non-crystalline but, by the use of radial distribution function (RDF) techniques, structural information can be obtained from X-ray diffraction data on materials of this type. The simplest and best characterised of the coating materials is aluminium phosphate, produced from a solution of a recently discovered complex with the formula $AlPO_4 \cdot HCl \cdot 4C_2H_5OH$. In the solid crystalline state, the structure of the complex has been shown to consist of cubic $AlPO_4$ tetramers which are prevented from linking up to form a long-range aluminium phosphate network by protonation of the non-bridging phosphate oxygens

and by ethanol ligands co-ordinated to the aluminium atoms [2].

The complex readily decomposes on heating to form amorphous $AlPO_4$.

$$AlPO_4 \cdot HCl \cdot 4C_2H_5OH = AlPO_4 + HCl + 4C_2H_5OH. \quad (1)$$

Coatings produced from solutions of the complex are, after heating, glassy continuous layers and this process is, in fact, the only known route to glassy $AlPO_4$. The crystal phases of $AlPO_4$ are closely similar to those of SiO_2 [3] and hence the vitreous forms of the two materials might be expected to have very similar structures. Vitreous silica has been well characterized using RDF methods [4]. Similar methods have been used in this investigation, to establish whether the RDF of vitreous $AlPO_4$ is quantitatively similar to that of vitreous silica, or whether some order of the complex precursor is preserved in the vitreous state. In the latter case the method of preparation might influence the resulting structure.

Two samples were examined, one being produced by direct decomposition of solid complex, the other by drying a solution of the complex in methanol and decomposing the solid obtained. The latter sample preparation route approximates closely to the way surface coatings are prepared in practice [1].

2. Experimental details and results

The experimental data collection system and the various correction procedures have been described in detail [5]. Samples for the diffraction experiments are required to be approximately 1 mm thick, but practical surface coatings are much thinner than this (typically $\sim 1\,\mu m$), and thus the samples were prepared as follows: sample 1 was produced by curing the solid complex at 200° C for 12 h followed by grinding the resulting solid to a fine powder and compacting this in a press to a circular plate 10 mm diameter and 1.0 mm thick. Sample 2 was produced from a 20% wt/wt solution of complex in methanol by blowing dry with nitrogen at room temperature followed by heating at 70° C for 6 h to remove any residual solvent and then curing at 200° C for 30 min. The resulting solid was then ground and compacted in the same way as for sample 1. The compacted plates were found to rapidly absorb water, and the equilibrium water contents at the time of collecting data were: sample 1, 8.7% wt/wt; sample 2, 12.0% wt/wt. These values were determined by thermogravimetric methods.

The data for sample 1 were collected using molybdenum radiation ($\lambda = 0.7107$ Å) and balanced filters on a constant time basis, spending a fixed time (15 min) for each filter (α and β). During the course of the work it was found that improved statistical accuracy, especially at high angles where count rates are low, could be obtained by collecting data on a constant count basis, i.e. measuring the time for a fixed count (10 000) using each filter. This procedure was subsequently adopted for sample 2 also using molybdenum radiation. Data were collected from $\theta = 0.5°$ to 66° at a fixed interval of 0.25°. The samples were positioned in the transmission scattering geometry [5]. The choice of collimation limits, methods of balancing the filters, collecting data at low scatter angles close to the incident beam, correcting for absorption in the sample, removing background scattering, and correcting for multiple scattering have already been described [5].

The data were converted to an equivalent constant time basis (sample 2), monochromatized by subtraction of the β counts from the α counts.

The sample intensity data were smoothed by fitting a second-order polynomial in θ to short segments of the scattering curve. This polynomial may be represented by the equation

$$[I_{sm}(\theta_i)]_r = (a_i)_r + (b_i)_r\theta_i + (c_i)_r\theta_i^2. \quad (2)$$

The coefficients a_i, b_i, and c_i were evaluated by a least squares method over an angular smoothing range designated by the subscript r. As indicated by the subscript i in the above equation, a separate set of coefficients is applicable to each value of the scattering angle and the value of I_{sm} corresponding to any given value of θ_i depends on the smoothing range selected. This angular smoothing range is given by the expression

$$(\theta_i - n\ \theta) \leqslant \theta \leqslant (\theta_i + n\ \theta)$$

where n is an integer and $\theta(= 0.25)$ is the angular spacing of the data points. Thus for each scattering angle, θ_i, the set of parameters a_i, b_i, and c_i were determined by using $2n + 1$ values of the sample intensity.

Several smoothing ranges were used to determine the complete scattering curve. These ranges were selected to include features that could be adequately represented by a second-order poly-

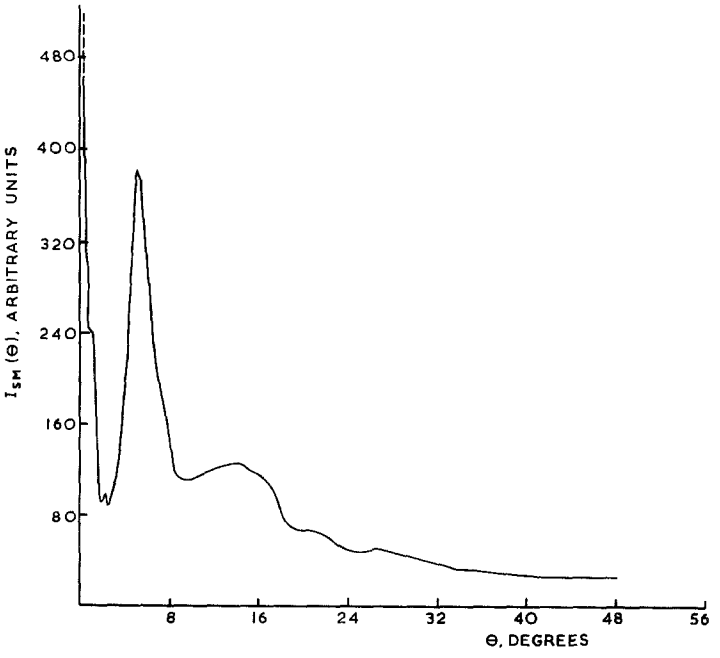

Figure 1 Scattered intensity for $AlPO_4$ prepared from solid $AlPO_4 \cdot HCl \cdot 4C_2H_5OH$ (sample 1).

nomial. In general, as the scattering angle increased and the intensity features became less prominent, a larger value of r was used. The following smoothing ranges were found to be satisfactory:

approximate angular region	smoothing range
$1° < \theta < 7°$	$n = 0, \theta_i$
$7° < \theta < 14°$	$n = 4, \theta_i \pm 1.0°$
$14° < \theta < 20°$	$n = 10, \theta_i \pm 2.5°$
$20° < \theta < 60°$	$n = 18, \theta_i \pm 4.5°$

Two separate smoothing computations were made for each sample. The purpose of the first smoothing was to obtain a preliminary estimate of the scattering curve. This preliminary estimate of $I_{sm}(\theta)$ was then used to statistically analyse the individual data points. To obtain the final estimate of the smooth scattering curve, a statistical analysis was made by computing a confidence interval about the preliminary estimate of $I_{sm}(\theta)$. In the experiment the true mean of $I(\theta)$ is unknown, and the best available estimate was $[I_{sm}(\theta)]_{prelim}$, since this curve was determined from a relatively large number of experimental observations. On this basis the preliminary value of $I_{sm}(\theta)$ was used to estimate the deviation of each point from the mean value. The standard deviation of each point was calculated using Gaussian statistics, and hence 95% confidence limits about the mean were constructed. Any experimental point falling outside these limits was labelled in the computer printout, and subsequently each labelled point was examined visually. The small number of labelled points which were obviously anomalous were removed and the smoothing computations were repeated to obtain a final estimate of the smooth scattering curve. The smoothed plot of $I_{sm}(\theta)$ for sample 1 is shown in Fig. 1, sample 2 giving a similar plot.

The data were normalized to electron units by plotting the normalization ratio:

$$N(\theta) = \frac{(1+B\theta)}{I_{sm}(\theta)} \left[\sum_{i=1}^{n} \frac{x_i f_i^2(\theta)}{a_c(\theta)} + \sum_{i=1}^{n} \frac{x_i I_{i(inc)}}{a_i(\theta)} \right] \quad (3)$$

against (θ), where B is a double scattering correction factor, n is the number of atomic species in the system, x_i is the atomic concentration of the ith species, f_i and $I_{i(inc)}$ are the dispersion corrected coherent scattering factors [6–9] and incoherent scattering factors [10–13] of the ith species, and $a_c(\theta)$ and $a_i(\theta)$ are the coherent and incoherent adsorption factors [5]. The normalization constant, C/NAT is given by,

$$\frac{C}{\text{NAT}} = \lim_{\theta \to \infty} \{N(\theta)\} \quad (4)$$

and was calculated by linearly averaging $N(\theta)$ between $28 \leqslant \theta \leqslant 50°$. Other methods of normalization together with their effect on the radial distribution function are discussed later in this section.

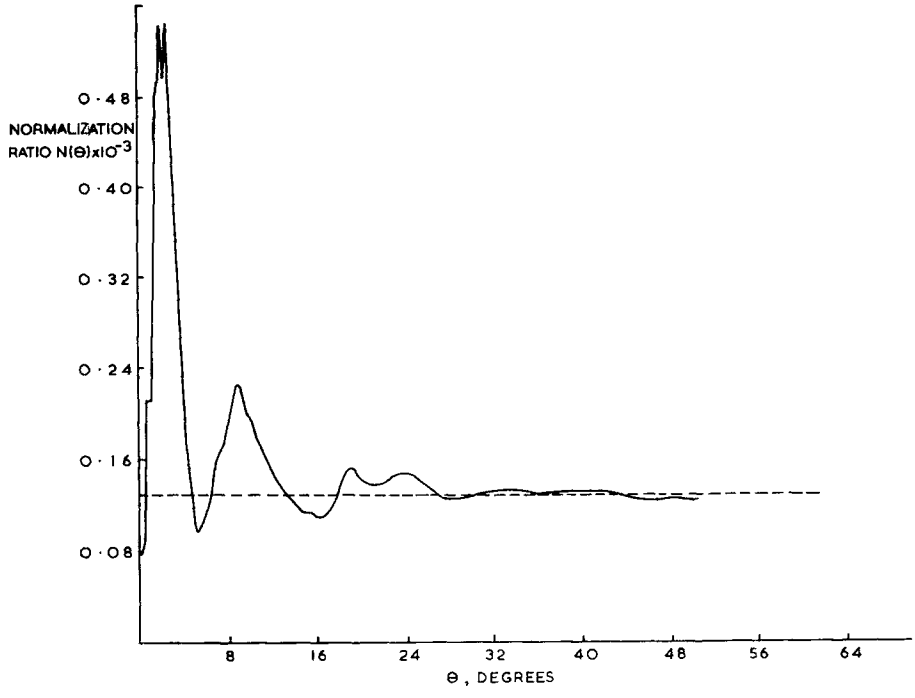

Figure 2 Normalization ratio for sample 1.

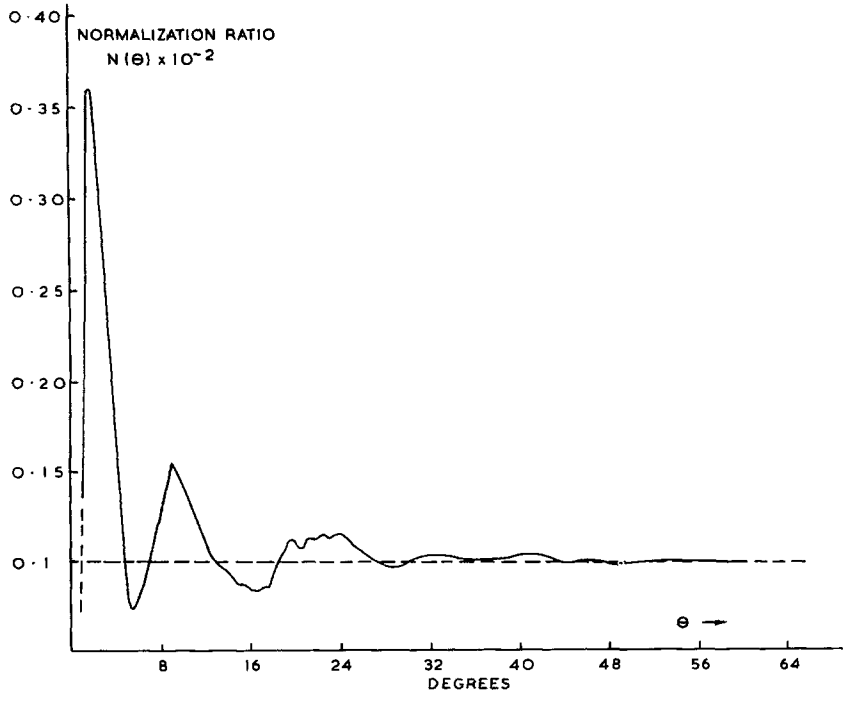

Figure 3 Normalization ratio for sample 2.

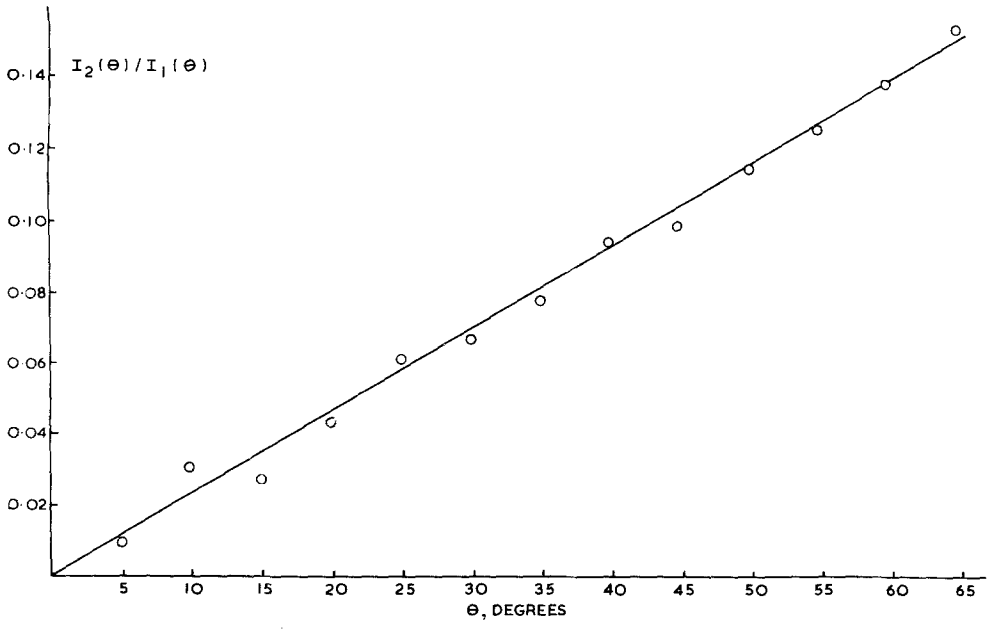

Figure 4 $I_2(\theta)/I_1(\theta)$ versus θ for sample 2.

Figs. 2 and 3 show the plots of $N(\theta)$ for sample 1 and 2, together with the values of B used in the analysis. It may be seen that the normalization ratio tends more closely to a constant value as $\theta \to \infty$ for sample 2 due to the better statistical accuracy for this sample. The drift away from a constant value at $\theta > 58°$ for sample 2 probably indicates the limitations of the linear multiple scattering correction term (Equation 3). The values of B used to correct for multiple scattering were checked by a computer calculation of the ratio of double scattering $I_2(\theta)$ to single scattering $I_1(\theta)$ as function of θ. This is shown in Fig. 5 for sample 2, using a finite element technique [14], based on the methods of Warren and Mozzi [15]. The irradiated volume of the sample and the potential secondary scattering are divided into finite elements and the double scattering is calculated by summation over all elements. The results tend to the correct value in the limit of infinitely fine elements, although this limit was not attainable in practice as the computing time became prohibitive. The results in Fig. 4 were calculated using volume elements of approximately $0.3 \times 0.3 \times 0.3\,\text{mm}^3$ with an irradiated volume of approximately $1.0 \times 1.0 \times 1.0\,\text{mm}^3$. The double scattering is given to a good approximation by,

$$I_2(\theta) \simeq BI_1(\theta) \tag{6}$$

or

$$I_{sm}(\theta) \simeq I_1(\theta) + I_2(\theta) \tag{7}$$

$$\simeq I_1(\theta)(1 + B\theta) \tag{8}$$

as assumed in the analysis. The value of $B = 0.0019$ compares favourably with the value of $B = 0.0039$ chosen empirically for the most favourable normalization behaviour for sample 2. On choosing an element size of $0.15 \times 0.15 \times 0.15\,\text{mm}^3$, B increased to 0.0025 when calculated for one scatter angle but further computation would not have been justified. Thus, in view of the neglect of third and higher order scattering terms which would presumably increase B further, the chosen method and numerical values adopted to perform a first order correction for multiple scattering are of the correct functional form, and of the correct order, within the limitations of the calculation techniques.

An average normalization constant $(C/\text{NAT})_{av}$ was chosen by averaging the values of Figs. 2 and 3 between $28 \leqslant \theta \leqslant 50°$ for each sample. An interference function, $J(\theta)$, defined by Wignall and Longman [5], was calculated from

$$j(\theta) = j(s) = 1.0 + \frac{\left\{\left[I_{sm}(C/NAT)_{av}/(1 + B\theta)\right] - \left[\sum_{i=1}^{n} x_i I^i \text{inc}/(a_i/\theta)\right] - \left[\sum_{i=1}^{n} x_i f_i^2(\theta)/(a_c(\theta)\right]\right\}}{\sum_{i=1}^{n} x_i f_i^2(\theta)}. \tag{9}$$

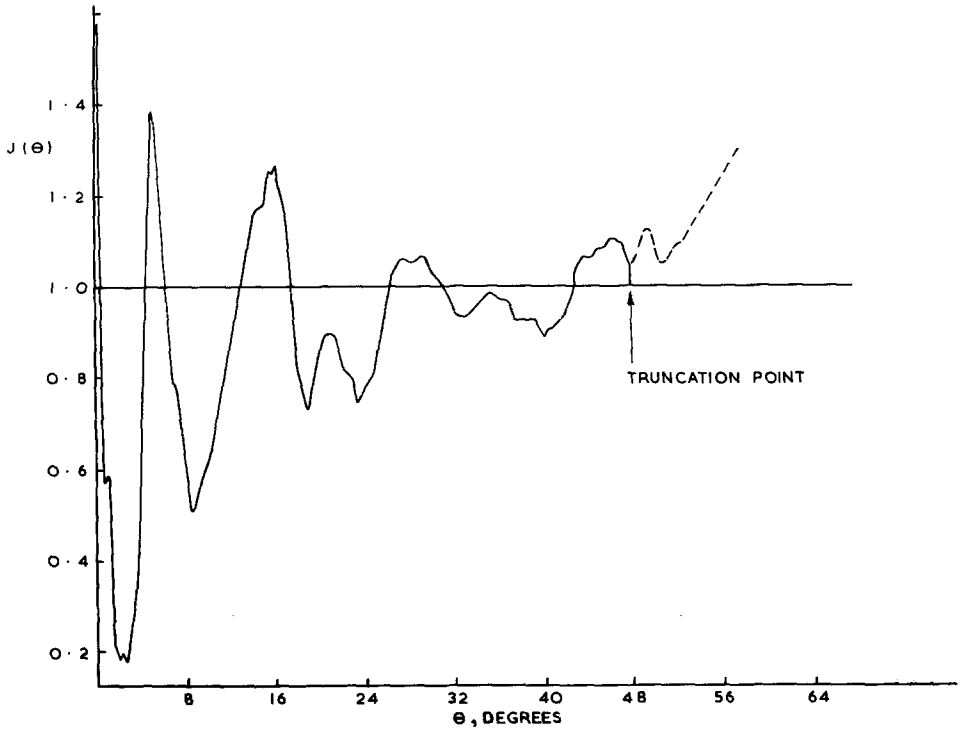

Figure 5 $J(\theta)$ versus θ for sample 1.

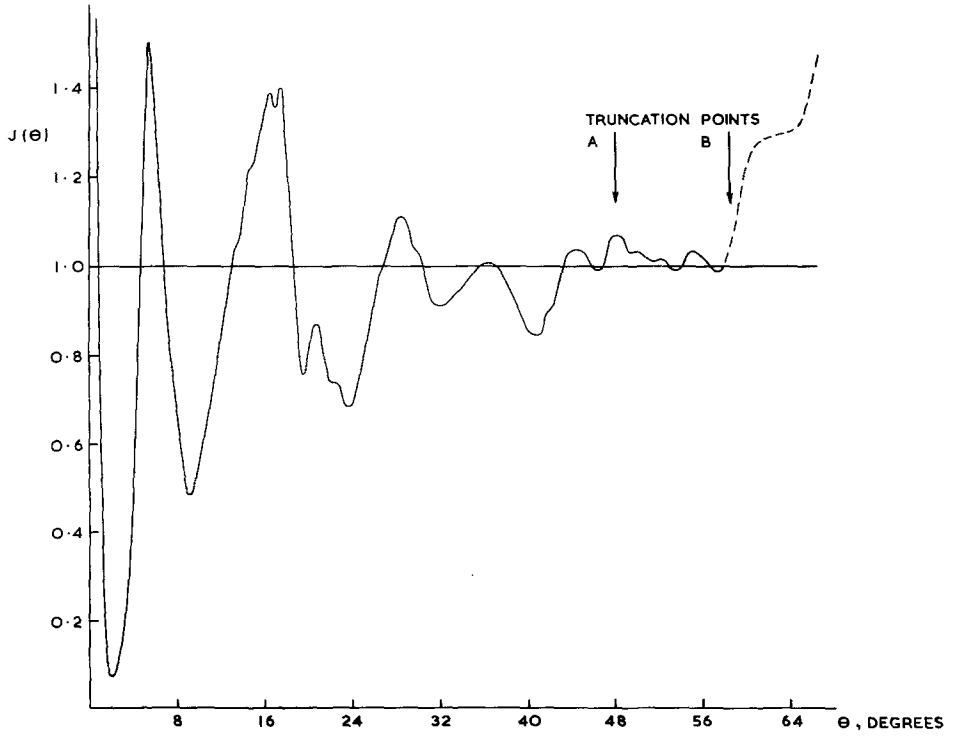

Figure 6 $J(\theta)$ versus θ for sample 2.

The interference functions are shown in Figs. 5 and 6 for samples 1 and 2 respectively. RDFs, $H(r)$, were calculated from,

$$H(r) = \frac{1}{2\pi^2 r\bar{\rho}} \int_{s=0}^{s_{max}} s\,[J(s) - 1] \sin sr\, ds \tag{10}$$

where $\bar{\rho}$ is the average atomic (number) density, $s = 4\pi \sin\theta/\lambda$ and s_{max} is the truncation limit of s.

The termination of data s_{max} can result in spurious oscillations in the radial distribution curve with a frequency $2\pi/s_{max}$, which may be reduced by increasing s_{max}. Alternatively, an exponential damping factor [5] may be applied to the data before transformation, although the latter approach results in some loss of resolution. No damping factor has been used in the present work as previous experience on the present experimental system has shown that truncation errors are small in the region $1 < r < 8$ Å. For example in the case of polyethylene, RDF plots obtained by the present system [16] and by electron diffraction [17] showed a large measure of agreement, despite a wide difference in truncation limits, s_{max}, used. Both sets of data gave peaks very close to the predicted short-range intra-molecular distances and the overall agreement confirms that truncation errors are not a major problem in this region of r space. A similar conclusion can be drawn from RDF studies on vitreous carbon [18].

In general the maximum value of θ was used at which the data was considered reliable. This is a subjective procedure, so the effect of terminating the data at two different values of θ (Fig. 6) was investigated for sample 2.

The RDFs for samples 1 and 2 are shown in Figs. 7 and 8 for truncation values of $s_{max} = 13.15\,\text{Å}^{-1}$. Fig. 9 presents the RDF for sample 2 with $s_{max} = 15\,\text{Å}^{-1}$ and shows essentially the same RDF as Fig. 8. Fig. 10 shows the sub-atomic region of $H(r)$. As this region is very sensitive to small errors in $J(s)$, the RDF exhibits spurious oscillations about its theoretical limit. Small differences in the method of normalization can have

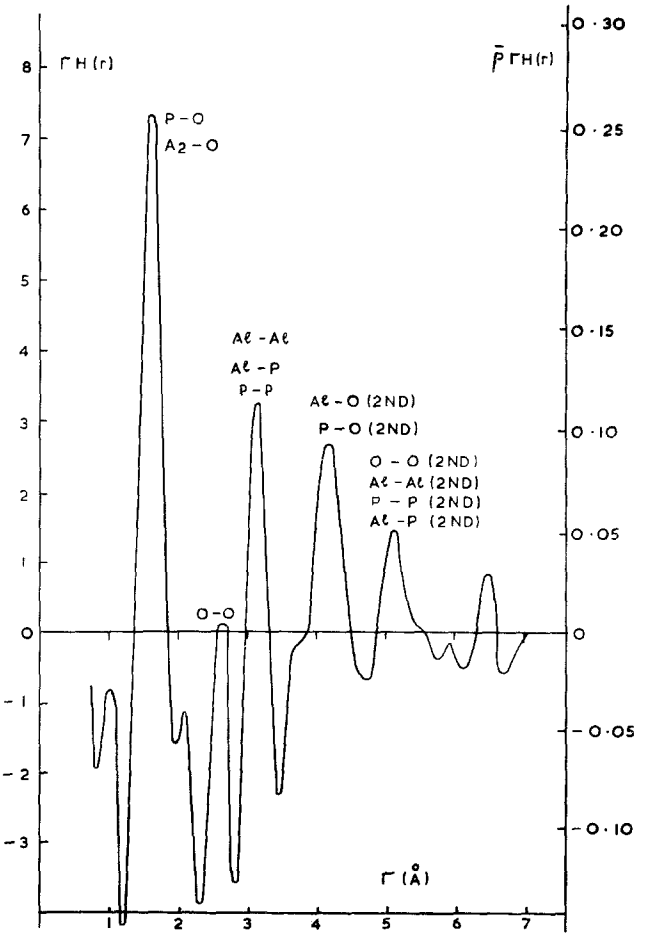

Figure 7 $rH(r)$ and $\bar{\rho}rH(r)$ versus r for sample 1.

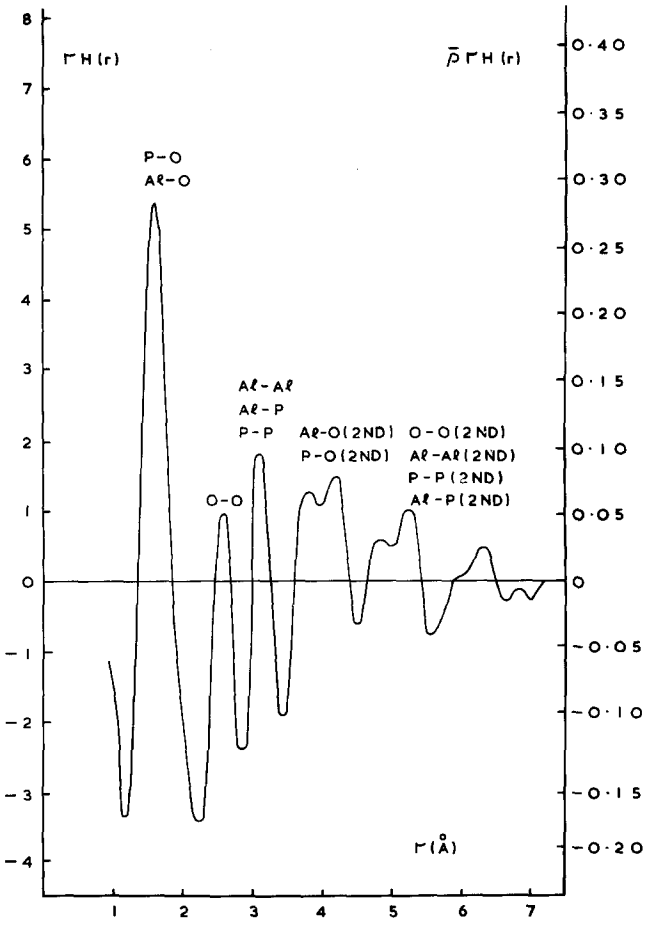

Figure 8 $rH(r)$ and $\bar{\rho}rH(r)$ versus r for sample 2 and truncation point A ($\theta = 48°$).

dramatic effects on the measured value of $H(0)$. Fig. 10 shows the results for the linear average method (used for Figs. 7 to 9) together with the results for a widely used alternative method [19]. Another method based on choosing a normalization constant to satisfy,

$$H(0) = -1 = \frac{1}{2\pi^2\bar{\rho}} \int_{s=0}^{s_{max}} s[J(s)-1]\,ds \tag{11}$$

as closely as possible is also shown. Equation 11 results from letting $r \to 0$ in Equation 10 and relies on the fact that $H(0)$ is -1 as atoms cannot pack at distances below $r \simeq 1$ Å. Hence by definition the atomic density is zero for very low r and $H(r) = -1$.

All sub-atomic oscillations are essentially non-physical due to the inability of atoms to pack at distances of < 1 Å. However, the dramatic effects of different normalization procedures are confined to sub-atomic distances as shown by Fig. 11 which illustrates the three different RDFs generated from the different normalization procedures. These are essentially identical for $r \geqslant 1.2$ Å.

3. Discussion

The RDF results for the samples of $AlPO_4$ produced from solid and the methanolic complex, presented in Figs. 7 and 8 respectively, show a remarkable similarity to the results of Mozzi and Warren [4] for vitreous silica (Fig. 12) when peak heights and shapes are compared. The peaks in the RDFs for $AlPO_4$ have been assigned to inter-atomic distances by analogy with the silica work. These assignments are included in Figs. 8 and 9 by comparison with the corresponding silica data in Fig. 12. Direct comparison of peak heights is not possible since Mozzi and Warren plot $r[H(r)+1]$ while Figs. 7 and 8 plot $rH(r)$. Comparison should only be made by measuring peak heights above the sloping baseline 0D in Fig. 12. However, it may then be seen that the peak heights are not in close agreement. This is probably due to the porous nature of the pressed $AlPO_4$ samples, since the measured average atomic densities were very low at 0.033 20 and 0.052 7 atoms Å^{-3} for samples 1 and 2 respectively. The difference between the two samples undoubtedly reflects differences in their pore

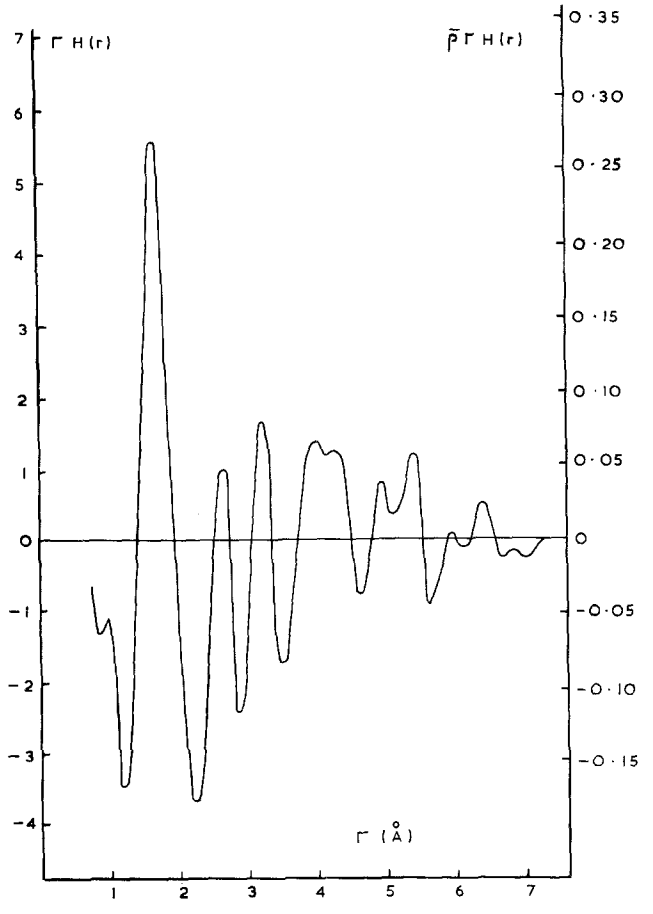

Figure 9 $rH(r)$ and $\bar{\rho}rH(r)$ versus r for sample 2 and truncation point B ($\theta = 58°$).

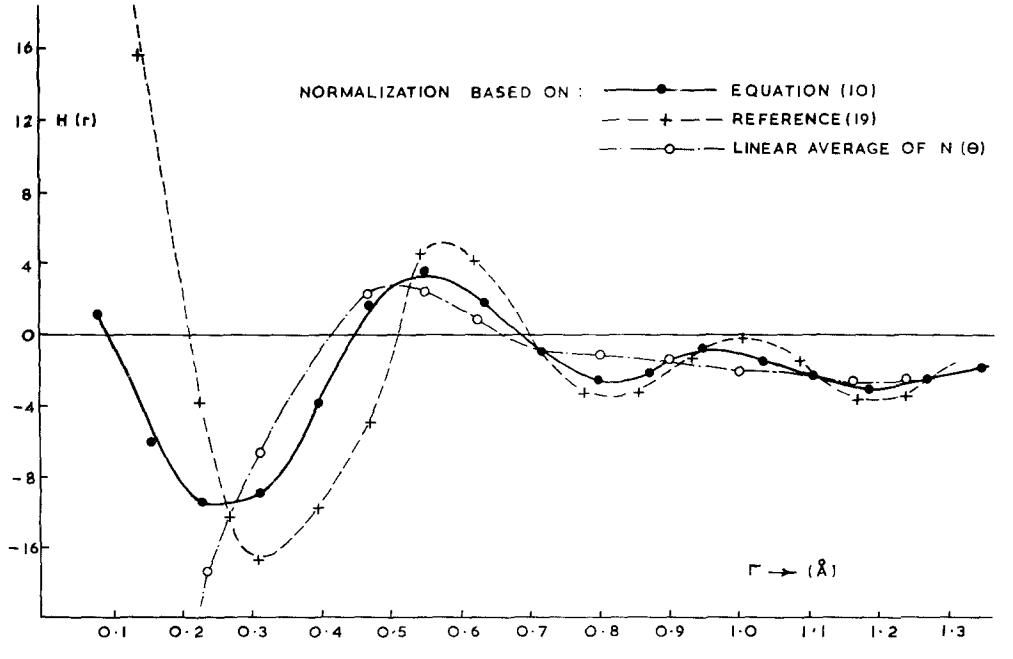

Figure 10 Sub-atomic behaviour of $H(r)$ for sample 2 and different normalization procedures.

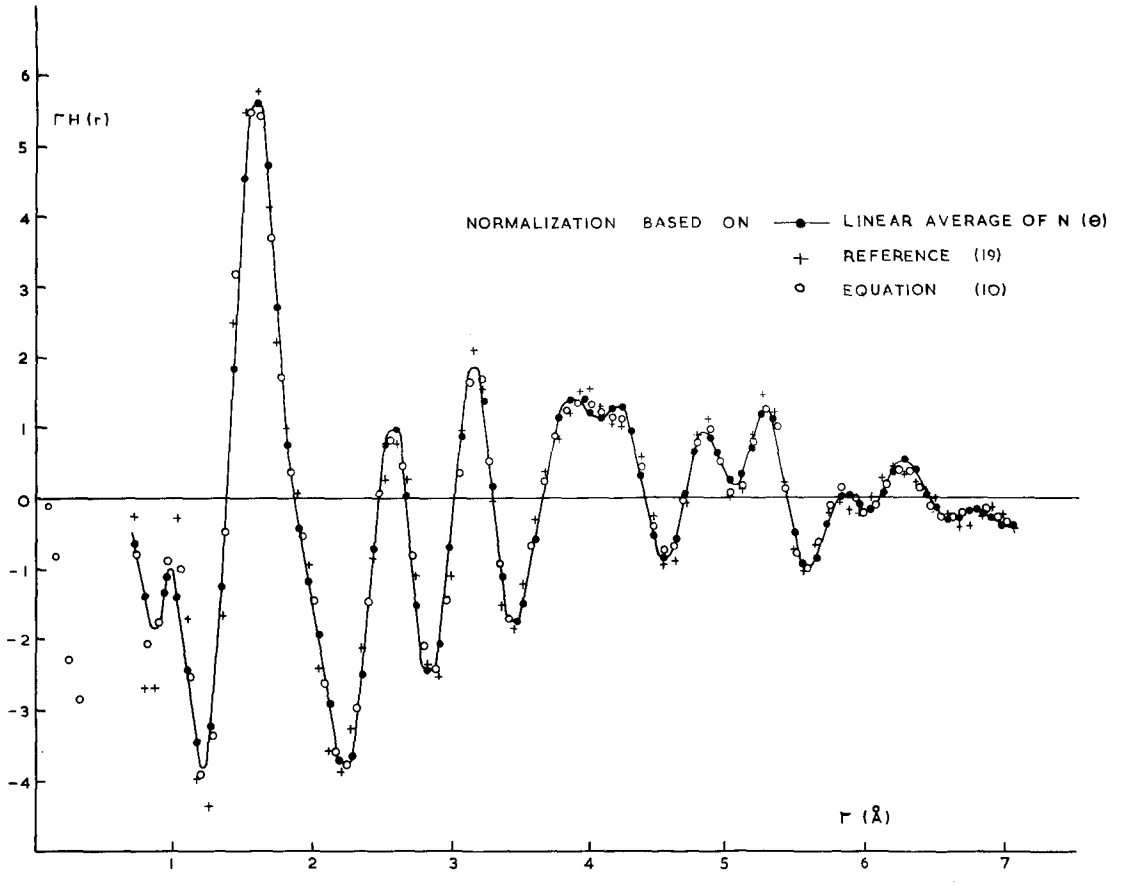

Figure 11 Effect of different normalization producedures on the RDF for sample 2.

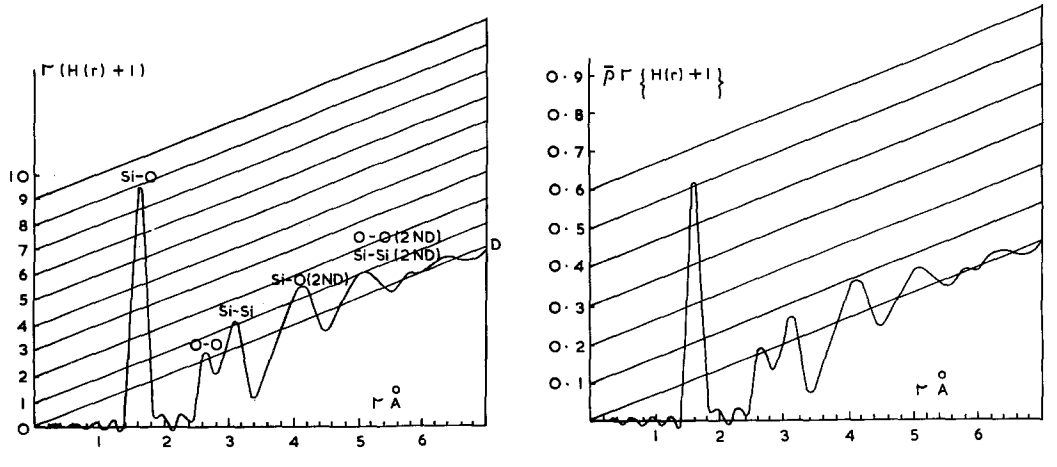

Figure 12 The RDF for silica [4].

volumes. Evidence of a porous structure can also be seen in the strong low angle scattering in Figs. 1, 5 and 6. To eliminate the density dependence, the right-hand axes of Figs. 7 and 8 have been plotted in terms of $\bar{\rho}rH(r)$, where

$$\bar{\rho}rH(r) = \frac{1}{2\pi^2}\int_{s=0}^{s_{max}} sJ(s)\sin sr\,ds. \quad (12)$$

It is then apparent that the peak intensities in the density independent RDFs of the two $AlPO_4$

samples are very similar. Comparison with the density independent RDF for silica (Fig. 12) shows that there is still a large difference in the height of the peak at ~ 1.6 Å. The probable explanation is that this peak represents the single nearest neighbour Si–O bond in silica [4] whereas for $AlPO_4$ it represents the summation of the P–O and Al–O bonds. These bonds have lengths of 1.53 and 1.8 Å, respectively [20], resulting in the observed broadening and reduction in peak height.

The co-ordination of the Al and P atoms can be estimated from the area of the 1.6 Å peak using the methods of Mozzi and Warren [4]. The peak area for SiO_2 is 2280 el^{2*} [4], whereas the peak area, taking a unit of composition of $AlPO_4$, for sample 2 is 1760 el^2 assuming tetrahedral co-ordination of oxygen atoms about both P and Al atoms. The agreement between these figures indicates that the assumption of four-fold co-ordination of network oxygen atoms is substantially correct, but the discrepancy of 500 el^2 indicates that absorbed water is also co-ordinated to the P and/or Al atoms with a P–O or Al–O distance of 1.6 Å. It is impossible to differentiate at this stage between co-ordination to Al or P atoms, although the discrepancy is of the correct order of magnitude to fit with the known moisture content (12%) of approximately one molecule of H_2O per $AlPO_4$ unit. Co-ordination of one molecule of H_2O per unit of composition to either Al or P would add 250 el^2 to the peak, and any other O–O co-ordination at a similar distance of 1.6 Å could make up the remaining discrepancy.

The RDFs for both $AlPO_4$ samples are very similar to that for SiO_2 although sample 2 shows slightly more order in the peaks at $r \sim 4$ and ~ 5 Å, indicating a more regular arrangement of the second neighbour distances. More exact comparison than this is not valid at this stage in view of the different water contents of the samples and the small (< 2 at. %) but undetermined amounts of chlorine and carbon present.

The similarity between the structure of vitreous $AlPO_4$ and vitreous silica is perfectly consistent with the crystal chemistry of $AlPO_4$, although the RDFs for vitreous $AlPO_4$ have been shown to differ slightly according to the route by which they were made. This indicates that the structure of the vitreous state depends on the method of preparation of the material.

Acknowledgements

The samples were prepared by R. J. Ashley and A. Wright. The authors also wish to acknowledge the help of Dr J. A. J. Jarvis in calculating the contribution of multiple scattering to the data.

References

1. R. N. ROTHON, *Chem. Ind.* June 1st (1974) 457.
2. J. E. CASSIDY, J. A. J. JARVIS and R. N. ROTHON, *J. Chem. Soc. (Dalton)* (1975) 1497.
3. J. R. VAN WAZER, "Phosphorus & it's Compounds", Vol. 1, Interscience, New York, 1966, p. 553.
4. R. L. MOZZI and B. E. WARREN, *J. Appl. Cryst.* 2 (1969) 164.
5. G. D. WIGNALL and G. W. LONGMAN, *J. Mater. Sci.* 8 (1973) 1439.
6. J. BERGHUIS, *et al. Acta Cryst.* 8 (1955) 478.
7. A. J. FREEMAN and R. E. WATSON, unpublished data.
8. A. J. FREEMAN, *Acta. Cryst.* **12** (1959) 261.
9. R. F. STEWART, E. R. DAVIDSON and W. T. SIMPSON, *J. Chem. Phys.* **42** (1965 3175.
10. D. T. CROMER and J. B. MANN, *J. Chem. Phys.* 47 (1967) 1892.
11. A. J. FREEMAN, *Phys. Rev.* **113** (1959) 169.
12. *Idem, Acta. Cryst.* **12** (1952) 929.
13. K. SAGEL, "Tabellen zur Rontgenstrukturenanalyse" (Springer Verlag, Berlin, 1958).
14. D. G. WIGNALL, J. A. J. JARVIS, W. E. MUNSIL and C. J. PINGS, *J. Appl. Cryst.* 7 (1974) 366.
15. B. E. WARREN and R. L. MOZZI, *Acta. Cryst.* **21** (1966) 459.
16. G. W. LONGMAN and G. D. WIGNALL, *Polymer* 17 (1976) 485.
17. I. VOIGT-MARTIN and F. C. MIJLHOFF, *J. Appl. Phys.* **46** (1975) 1165.
18. G. D. WIGNALL and C. J. PINGS, *Carbon* **12** (1974) 51.
19. J. KROGH-MOE, *Acta Cryst.* **1** (1958) 267.
20. "International Tables for X-ray Crystallography", Vol. 3 edited by C. H. MacGillavry and G. D. Rieck (Kynoch Press, Birmingham, 1962).

Received 20 January and accepted 27 August 1976.

*el^2 is an abbreviation for (electron)^2 which are units of peak area, each peak being attributed to one or more bonds or interatomic distances.